Nuclear stopping and rapidity loss in Au+Au collisions at $\sqrt{s_{NN}}$=62.4 GeV

I.C.Arsene[k], I.G.Bearden[f], D.Beavis[a], S.Bekele[j], C.Besliu[i], B.Budick[e], H.Bøggild[f], C.Chasman[a],
C.H.Christensen[f], P.Christiansen[f,3], H.H.Dalsgaard[f,*], R.Debbe[a], J.J.Gaardhøje[f], K.Hagel[g], H.Ito[a], A.Jipa[i],
E.B.Johnson[j,1], C.E.Jørgensen[f], R.Karabowicz[d], N.Katrynska[d], E.J.Kim[j,2], T.M.Larsen[f], J.H.Lee[a],
G.Løvhøiden[k], Z.Majka[d], M.J.Murray[j], J.Natowitz[g], B.S.Nielsen[f], C.Nygaard[f], D.Pal[j], A.Qviller[k],
F.Rami[1], C.Ristea[f], O.Ristea[i], D.Röhrich[h], S.J.Sanders[j], P.Staszel[d], T.S.Tveter[k], F.Videbæk[a,5],
R.Wada[g], H.Yang[h], Z.Yin[h,4], I.S.Zgura[c]

[a]*Brookhaven National Laboratory, Upton, New York, USA*
[b]*Institut Pluridisciplinaire Hubert Curien,IN2P3-CNRS et Université Louis Pasteur, Strasbourg, France*
[c]*Institute of Space Science,Bucharest-Magurele, Romania*
[d]*M. Smoluchowski Inst. of Physics, Jagiellonian University, Krakow, Poland*
[e]*New York University, New York, USA,*
[f]*Niels Bohr Institute, University of Copenhagen, Copenhagen, Denmark*
[g]*Texas A&M University, College Station, Texas, USA*
[h]*University of Bergen, Department of Physics and Technology, Bergen, Norway*
[i]*University of Bucharest, Romania*
[j]*University of Kansas, Lawrence, Kansas, USA*
[k]*University of Oslo, Department of Physics, Oslo, Norway*

Abstract

Transverse momentum spectra of protons and anti-protons measured in the rapidity range $0 < y < 3.1$ from 0-10% central Au+Au collisions at $\sqrt{s_{NN}} = 62.4$ GeV are presented. The rapidity densities, dN/dy, of protons, anti-protons and net-protons $(N_p - N_{\bar{p}})$ have been deduced from the spectra over a rapidity range wide enough to observe the expected maximum net-baryon density. From mid-rapidity to $y = 1$ the net-proton yield is roughly constant $(dN/dy \sim 10)$, but rises to $dN/dy \sim 25$ at $2.3 < y < 3.1$. The mean rapidity loss is $2.01 \pm 0.14 \pm 0.12$ units from beam rapidity. The measured rapidity distributions are compared to model predictions. Systematics of net-baryon distributions and rapidity loss vs. collision energy are discussed.

PACS numbers: 25.75 Dw.

In collisions between gold nuclei at the top energy ($\sqrt{s_{NN}} = 200$ GeV) of the Relativistic Heavy Ion Collider, RHIC, there is strong evidence of a state of matter characterized by partonic (quark and gluon) degrees of freedom and with properties similar to that of a nearly perfect liquid [1, 2, 3, 4, 5]. The partons are produced copiously during the initial stages of the collisions and subsequently hadronize into the roughly 7000 [6] particles produced in central collisions. The energy required for producing these particles comes from the kinetic energy lost by the baryons in the colliding nuclei. Since $E = m_T \cosh y$, where

$m_T = \sqrt{m^2 + p_T^2}$ is the transverse mass (p_T is the transverse momentum), and y is the rapidity, this energy loss is manifest as a loss in mean rapidity of these baryons.

The net-baryon yield can be estimated from the net-proton yield, which is taken as the difference between the measured yields of protons and anti-protons. The rapidity distribution of the net–protons after the collision then not only determines the energy available for particle production, but also yields information on the stopping of the ions due to their mutual interaction.

By having a measurement at an energy between the lower energy AGS ($\sqrt{s_{NN}} = 5$ GeV) and SPS ($\sqrt{s_{NN}} = 17$ GeV) data and the highest energy RHIC results ($\sqrt{s_{NN}} = 200$ GeV) [7, 8, 9], the development of rapidity and energy loss can be studied in greater detail. In this Letter, we present the first measurements of the rapidity loss of Au ions after central collisions at $\sqrt{s_{NN}} = 62.4$ GeV. The experimental arrangement of the BRAHMS detector at RHIC makes it possible to measure the distribution of net-protons

---

*Corresponding Author.
e-mail address: canute@nbi.dk(H.H.Dalsgaard)
[1]Present address: Radiation Monitoring Devices, Cambridge, MA, USA
[2]Present address: Division of Science Education, Chonbuk National University, Jeonju, Korea
[3]Present Address: Div. of Experimental High-Energy Physics, Lund University, Lund, Sweden
[4]Present Address: Institute of Particle Physics, Huazhong Normal University,Wuhan,China
[5]Spokesperson *e-mail: videbaek@bnl.gov*

over a rapidity interval $y = 0$ to $y = 3.1$. This rapidity range is wide enough to include the maximum proton rapidity density, in contrast to the situation at the RHIC top energy, where the beam rapidity is higher ($y_b = 5.4$ compared to 4.2 at 62 GeV) and where the acceptance of existing experiments does not include this peak. The situation at the lower energy therefore makes it possible to better determine the rapidity density distribution. Together with similar information from experiments at lower energies, and at the RHIC top energy, we conclude that the mean rapidity loss of ultra-relativistic heavy ions exhibits a slowly varying behavior as a function of beam energy from SPS energies on upwards.

The BRAHMS detector consists of two magnetic spectrometers: the Mid Rapidity Spectrometer (MRS) able to cover polar angles (measured with respect to the beam direction) $30° < \theta < 90°$ and the Forward Spectrometer (FS) able to cover $2.3° < \theta < 15°$. Each spectrometer determines trajectories and momenta of charged hadrons. Two Time Projection Chambers (TPCs) are utilized in the MRS and two TPCs and three Drift Chambers (DCs) in the FS. Together, they measure protons and anti-protons in the range $-0.1 < y < 3.5$. Collision centrality is determined using a silicon and plastic tile multiplicity array located around the nominal intersection point (NIP) [6]. For this analysis, the centrality class $0 - 10\%$ was selected, corresponding to a calculated number of participant nucleons of $N_{part} = 314 \pm 8$. The vertex position is determined with an accuracy of ≈ 1 cm using two arrays of Cherenkov counters positioned on either side of the NIP [10]. We have selected for analysis tracks in the MRS (FS) with vertices within $\pm 15(20)$cm from the NIP.
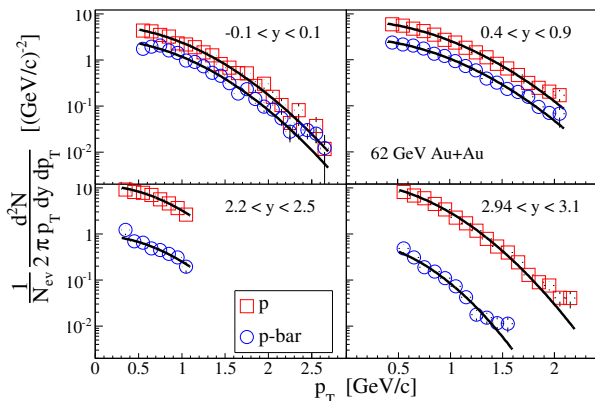
Figure 1: Spectra of identified protons and anti-protons for $y \sim 0$, $y \sim 0.65$, $y \sim 2.3$ and $y \sim 3$ respectively. The solid drawn lines are the fit functions used to determine the yield. Vertical bars show statistical errors only.

Particle identification (PID) is done in the MRS via time of flight (TOF) measurements, enabling clean identification of protons and anti-protons in the mo-

mentum range $0.4 < p < 3$ GeV/c.

In the FS, two PID detectors are used: A TOF system and a Ring Imaging Cherenkov (RICH) detector. In the RICH, only (anti-)protons with $p > 15$ GeV/c can create resolvable rings. Lower momentum (anti)protons have no associated Cherenkov radiation. In this letter we have two sets of FS data corresponding to two settings of the spectrometer which again corresponds to rapidities $y \sim 2.3$ and $y \sim 3$. For $y \sim 2.3$ we use use the TOF for PID with the RICH as a veto detector. In the momentum range $3 < p < 7.5$ GeV/c we apply a 2 sigma cut about the (anti-) proton peak in the calculated mass spectrum based on the TOF measurement and require that the particle not be identified in the RICH as a pion. For $y \sim 3$ the RICH is used exclusively for PID in the momentum range $10 < p < 30$ GeV/c. For $15 < p < 30$ GeV/c we make a 2 sigma cut around the peak in the mass spectrum calculated from the ring radii. If there is no resolvable ring we select particles that fail to make rings so that for $10 < p < 17$ GeV/c the (anti)protons are those particles with either no associated ring or a ring with a small radius. There is an overlap in momentum to catch (anti)protons that fail to create a ring despite momenta of $p > 15$ GeV/c.

The timing resolution of the MRS TOF is 90 ± 5 ps and the timing resolution in FS is 95 ± 6. The momentum resolution in FS is $\Delta p/p = 0.016 \cdot p/p_{ref}$ where p_{ref} is the reference momentum for a given field setting. At the 1/2 field where the $y \sim 3$ data were taken $p_{ref} = 11$ GeV/c. Overall the $\Delta p/p$ is 1-2% for all settings in FS. For the MRS $\Delta p/p \sim 0.014p$ at large p [11].

The differential invariant yields, $\frac{1}{2\pi p_T} \frac{d^2N}{dydp_T}$, of protons and anti-protons have been corrected for geometrical acceptance and detector efficiency. The acceptance correction is, due to the small solid angle of the BRAHMS spectrometers, the largest correction and is obtained from a purely geometrical simulation of each combination of angle and magnetic field used in the experiment. The PID efficiency of the TOF walls is found to be 93-98%. Since the RICH is 97% efficient for particles above threshold, up to 3% of pions and kaons in the momentum range 10 GeV/$c < p < 17$ GeV/c with ring radii zero will be mistakenly identified as protons, an effect for which we correct the data. This is done by first creating a spectrum of (anti)kaons and (anti)pions as if they were (anti)protons. Then we subtract 3% of this spectrum from the (anti)proton spectrum. The correction to protons is small, while for p-bar it amounts for up to 50% of the yield. Since the p-bar yield is small the effect on the net-protons is small. The total tracking efficiency in the MRS and FS is $\approx 90\%$ and $\approx 80\%$, respectively. The data have also been corrected for absorption, energy loss and multiple scattering esti-
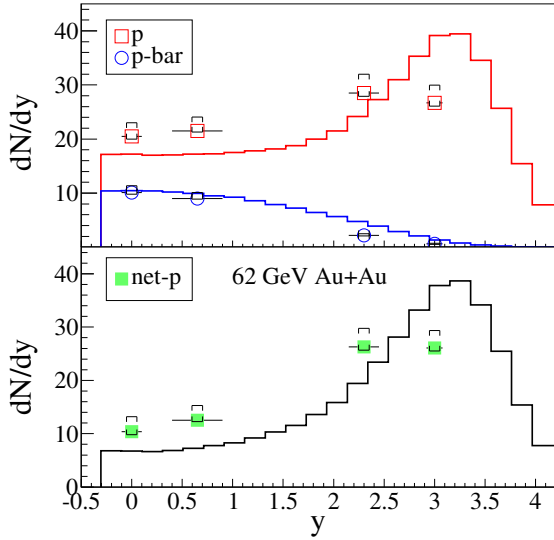
Figure 2: Top: rapidity densities of protons and anti-protons. Bottom: rapidity densities of net protons. The statistical errors are smaller than the marker sizes. The vertical brackets shows the estimated systematic errors due the extrapolation of yields, and the horizontal bars indicate the width of the rapidity interval for each data point. The histograms are from HIJING/BB̄(v2.1).

mated through simulations using GEANT [12]. The corrections for these physics effects amount to less than 20% at the lowest p_T and less than 15% at the highest p_T for the FS, whereas in the MRS the correction at the highest p_T is $\approx 8\%$.

Fig. 1 shows the invariant spectra of protons and anti-protons for $y \sim 0$, $y \sim 0.65$, $y \sim 2.3$ and $y \sim 3$ as a function of p_T. The integrated yields have been obtained by fitting these spectra with Gaussian functions ($f(p_T) \propto exp(-p_T^2/2\sigma^2)$) and integrating the fit functions in the range $0 < p_T < \infty$. From the yields we obtain the rapidity densities $\frac{dN}{dy}$. The integrated yield under the data points compared to the extrapolated yield is $\sim 80 - 90\%$ in the MRS and $\sim 40 - 50\%$ in the FS. The mean p_T and m_T determined from the distributions varies from $\langle p_T \rangle \sim 1$ GeV/c ($\langle m_T \rangle \sim 1.4$ GeV) in the MRS to $\langle p_T \rangle \sim 0.7$ GeV/c ($\langle m_T \rangle \sim 1.2$ GeV)in the FS. The fits represent the data well. The spectra and the fits are consistent within 5% in the covered regions in p_T.

The top panel of Fig. 2 shows the dN/dy of protons and anti-protons. The lower panel shows the dN/dy of the net-protons, defined here as the difference of the protons and anti-proton densities. The systematic errors due to the limited p_T coverage have been found to be less than 7%. The main source of systematic uncertainties comes from the choice of fit function. We have used two alternative fit functions, a Boltzmann

in m_T and an exponential in m_T, to estimate this systematic error. By varying the choice of fit functions we have found that this systematic error is less than 10 %. Since both the alternative fit functions give higher yields than the Gaussian in p_T this systematic error is asymmetric, ie. only positive. These uncertainties together with those for the corrections results in an estimate of the total systematic error of roughly 12%.

The predictions of the HIJING/BB̄(v2.1) event generator [13] for the proton, anti-proton and net-proton rapidity distributions are shown in Fig. 2 by the histograms. The HIJING distributions include protons and anti-protons from hyperon decays that would be measured as primary protons (e.g. 0.53 ± 0.05 (anti-)protons for each (anti-)lambda, see [9]). The HIJING calculation predicts a smaller net-proton yield at mid-rapidity, and shows a peak slightly forward of that indicated by our results; thus, the mean rapidity loss is smaller than estimated from our data.

The estimate for net-baryons depends on the relative acceptance for direct and decay protons in the spectrometers and the ratio of hyperons to protons. The acceptances are calculated using GEANT while the hyperon:proton ratios have been calculated using the THERMUS [14] model. The THERMUS results are based on fits to BRAHMS $\pi^{\pm}, K^{\pm}, p$ and $\bar{p}$ data [15]. The necessary conversion from the net-protons, $\frac{dN_{p-\bar{p}}}{dy}$, to the net-baryons, $\frac{dN_{B-\bar{B}}}{dy}$, is then done (similar as in Ref. [9], neglecting the contribution from Σ) as:

$$\frac{dN_{B-\bar{B}}}{dy} = \frac{dN_{p-\bar{p},meas}}{dy} \frac{n_p + n_n + n_\Lambda}{n_p + c_1 n_\Lambda} \qquad (1)$$

Here $\frac{dN_{p-\bar{p},meas}}{dy}$ is the number of measured protons, n_p is the true number of protons, n_n is the number of neutrons and n_{Lambda} is the number of Λ. The constant c_1 is the contribution from weak decays of Λ particles and has been estimated using MC simulations to be $c_1 = 0.53 \pm 0.05$ [9]. The n/p ratio is obtained from HIJING. The Λ/p ratios have been calculated from THERMUS [14]. Using Eq. 1 we obtain $\frac{dN_{B-\bar{B}}}{dy} = (2 \pm 0.1) \cdot \frac{dN_{p-\bar{p}}}{dy}$ at mid-rapidity and $\frac{dN_{B-\bar{B}}}{dy} = (2.1 \pm 0.1) \cdot \frac{dN_{p-\bar{p}}}{dy}$ at forward rapidities (the larger correction at forward rapidity is due to a small increase in the n/p ratio at forward rapidities).

We quantify the mean rapidity [16] and energy loss using the following integrals:

$$\delta y = y_b - \frac{2}{N_{part}} \int_0^{y_b} y \frac{dN_{B-\bar{B}}}{dy} dy \qquad (2)$$

$$\delta E = E_b - \frac{2}{N_{part}} \int_0^{y_b} \langle m_T \rangle \cosh y \frac{dN_{B-\bar{B}}}{dy} dy. \qquad (3)$$

Here y_b and E_b are the rapidity and energy of the incoming beams and $dN_{B-\bar{B}}/dy$ is the net-baryon rapidity density. Since we only have data at four rapidities, $y = 0, 0.65, 2.3$ and 3, we have to both interpolate

and extrapolate our data to evaluate the integrals. We found that $\langle m_T \rangle$ drops linearly with rapidity. For the baryon yield we fitted our data to a $3^{\rm rd}$ order polynomial in y^2 (analogous to [9]) subject to the constraint that $N_{part} = 314$ and that the yield at y_b is 0. The result of this fit together with our net-baryon distribution are shown in the inset of Fig. 3.

Using this method we obtain the average rapidity and energy loss per participant baryon for Au+Au collisions at $\sqrt{s_{NN}} = 62.4$ GeV (stat. + syst. error):

$$\delta y = 2.01 \pm 0.14 \pm 0.12, \quad \delta E = 21.1 \pm 1.6 \pm 2.8 \text{ GeV}.$$

Since the energy loss per pair of participant nucleons is $2\delta E$, approximately 70% of the initial beam energy is available for particle production and longitudinal and transverse momentum. Applying the conversion from net–protons to net–baryons and fitting the result, we estimate that for collisions with $N_{part} \sim 314$, there are ~ 240 net–baryons in the acceptance covered by BRAHMS, $-3.1 < y < 3.1$ (because of symmetry). To estimate the minimum and maximum possible stopping at $\sqrt{s_{NN}} = 62.4$ GeV the remaining baryons can be placed at $y = 3.1$ or $y = y_b$. The minimum and maximum rapidity loss are found to be $\delta y = 1.85$ and $\delta y = 2.11$ respectively whereas the minimum and maximum energy loss are found to be $\delta E = 18.4$ GeV and $\delta E = 24.1$ GeV. Using these numbers we have estimated the systematic errors on the stopping and energy loss.
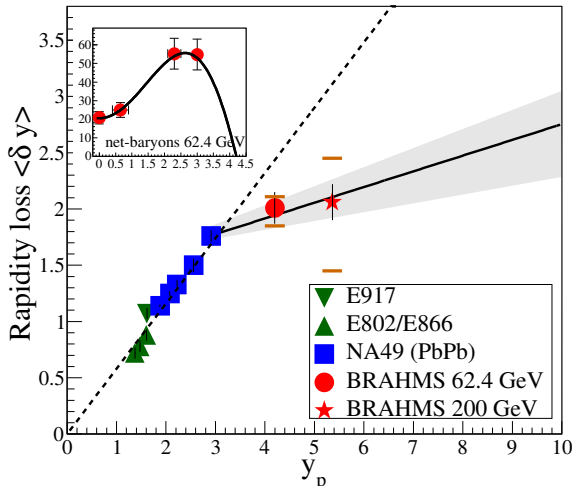
Figure 3: Rapidity losses for heavy systems (Au,Pb) from AGS, SPS and RHIC as a function of beam rapidity. The solid line is a fit to SPS and RHIC data, and the band is the statistical uncertainty of this fit. The LHC beam rapidity is $y = 8.67$. The dashed line is a linear fit to AGS and SPS data from [16]. The lower rapidity points from NA49 are preliminary data from [17].

The rapidity losses at AGS [7, 18, 19], SPS [8] and RHIC $\sqrt{s_{NN}} = 200$ GeV [9] together with the present

result are summarized in Fig. 3. The figure shows that rapidity loss increases rapidly with beam energy from AGS to SPS but much more slowly from SPS energy to RHIC energies. The dotted line in Fig. 3 is taken from [16] where there was found to be a linear scaling over a wide range of energies up to the SPS top energy. This scaling was found to be broken at $\sqrt{s_{NN}} = 200$ GeV in [9] and we conclude that the proposed linear scaling breaks between $\sqrt{s_{NN}} = 17$ GeV and $\sqrt{s_{NN}} = 62.4$ GeV. The solid drawn line is a linear fit to SPS and RHIC data and allows one to extrapolate to the LHC regime ($y_b = 8.67$). The grey band gives the statistical uncertainty of this extrapolation, but is only useful to the extent that the underlying physics is the same from RHIC to LHC energies.
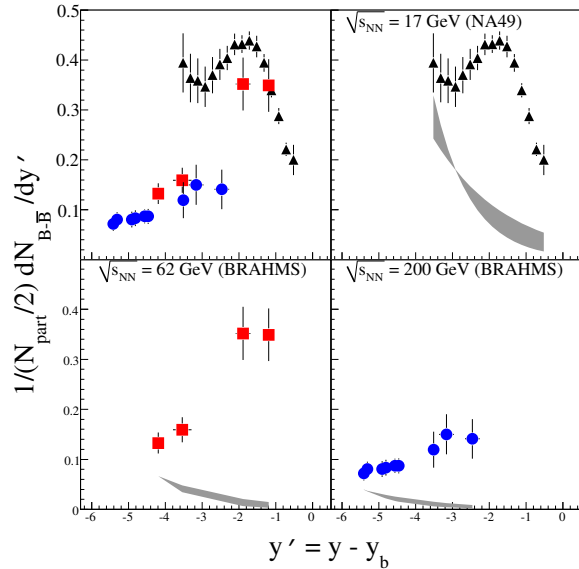
Figure 4: The top left panel shows $(1/N_{part}/2)dN_{B-\bar{B}}/dy'$ where $y' = y - y_b$ for SPS and RHIC energies. No scaling is observed. The three other panels show data from SPS and RHIC drawn together with the 'target' net-baryon contribution from [21]. The triangles represent data from NA49, the squares BRAHMS data from 62 GeV and the circles BRAHMS 200 GeV data.

Horizontal bars in Fig. 3 are the extremes of the the 62.4 GeV stopping as discussed above. The horizontal bars for the $\sqrt{s_{NN}} = 200$ GeV are obtained in the same way, and similarly give the absolute limits on the amount of stopping. If instead of relying on these limits, we use the uncertainty on the fits to the yields to perform the extrapolation to LHC, we then find that the rapidity loss at LHC would be expected to lie between $2.1 < \delta y < 2.8$.

The slow increase of the rapidity loss from the top SPS energy to the top RHIC energy indicates that baryon transport does not depend strongly on energy at high energies when observed in the rapidity frame of the beam, $y' = y_{CM} - y_b$. We therefore compare dN/dy' for net-baryons normalized to the number of

4

participant pairs. For NA49 data [8] the number of net-baryons is 352 ± 12 for the interval $|y_{cm}| < 2.5$. Extrapolating to $y_b = 2.9$ we estimate the number of participants to be 390 ± 20.

Fig. 4 (top left) shows net-baryon rapidity densities $1/(N_{part}/2)dN_{B-\bar{B}}/dy'$ for different beam energies. The $\sqrt{s_{NN}} = 17$ GeV and $\sqrt{s_{NN}} = 62.4$ GeV data differ significantly at $y' \sim -3$ but approach each other towards y_b, coinciding at $y' \sim -1$, reflecting the much larger contribution of 'target' baryons at $\sqrt{s_{NN}} = 17$ GeV. This is reminiscent of limiting fragmentation and indeed is the reason for choosing the variable y'.
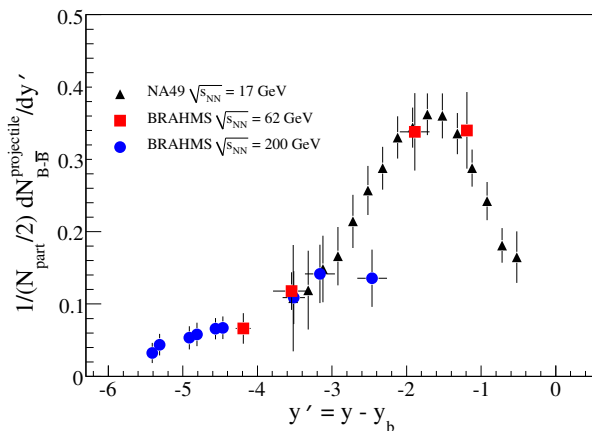
Figure 5: Projectile net-baryon rapidity density $(1/N_{part}/2)dN_{B-\bar{B}}^{projectile}/dy'$ from SPS and RHIC after subtraction of the target net-baryon contribution (see Fig. 4).

This direct comparison of data is complicated by the aforementioned target contribution. For $\sqrt{s_{NN}} = 17$ GeV at $y' = -3$ the target contribution is half the net-baryons while for $\sqrt{s_{NN}} = 62.4$ GeV and $\sqrt{s_{NN}} = 200$ GeV the contribution is significantly less. To compare the net-baryons from the projectile only, the target contribution must be subtracted. At $y_{CM} = 0$ the target nucleons comprise half of the net-baryons due to beam-target symmetry, and at y_b the target contribution is expected to be negligible. Between these extremes we consider two different rapidity dependences for the correction: (1) a simple exponential form $\exp(-y')$ [20] and (2) a gluon junction motivated form $\exp(-y'/2)$ [21]. These two functions give limits for the target net-baryon tail and provide the bounds for the grey bands in Fig. 4. We subtract the average of these two functions, with half the difference between them taken to be the systematic uncertainty on the function, from the data. A consequence of the forward-backward (beam-projectile) symmetry is that there is no error on the beam contribution at mid–rapidity. As one approaches the projectile rapidity, the uncertainty grows, but both the absolute and relative contribution of the target net-

baryons decreases and the correction becomes smaller. After subtracting the target net-baryon contribution shown in Fig. 4, we obtain the projectile net-baryon distributions presented in Fig. 5. One notes a remarkable similarity among the data sets for large rapidity losses $y' < -3$, while the 200 GeV data may begin to diverge from the lower energy data for $y' > -3$. This suggests that the rapidity loss obtained from Eq. 1, which does not distinguish the target and projectile contributions to the net-baryon yield, while experimentally practical, is slightly misleading, and that the increase in projectile rapidity loss from SPS to RHIC maximum energy might be smaller than what is implied in Fig. 3.

Finally, we note that the present results for the rapidity loss of baryons(protons) for Au+Au collisions at $\sqrt{s_{NN}} = 62.4$ GeV, together with similar data at lower and higher energy permit us to more accurately determine the onset of a collision regime where the absolute rapidity loss appears to vary slowly with beam rapidity, with the data exhibiting a near saturation of the rapidity loss with increasing collision energy. Recently, it has been argued [22] that such a scaling may result from gluon saturation of the collision. These results suggest that the rapidity loss at LHC will be approximately $\delta y = 2.3$. Although the baryon rapidity loss relative to the beam rapidity decreases, the overall energy available for particle production still increases with increasing beam energy.

References

[1] I. Arsene et al., BRAHMS Collaboration, Nucl. Phys.A 757 (2005) 1.

[2] J. Adams et al., STAR Collaboration, Nucl. Phys.A 757 (2005) 102.

[3] K. Adcox et al., PHENIX Collaboration, Nucl. Phys.A 757(2005)184.

[4] B.B. Back et al., PHOBOS Collaboration, Nucl. Phys.A 757 (2005) 28.

[5] M. Gyulassy and L. McLerran, Nucl. Phys.A 750 (2005) 30.

[6] I.G. Bearden et al., BRAHMS Collaboration, Phys. Rev. Lett.88 (2002) 202301 (2002).

[7] B.B. Back et al., E917 Collaboration, Phys. Rev. Lett.86 (2001) 1970.

[8] H. Appelhäuser et al., NA49 Collaboration, Phys. Rev. Lett.82 (1999) 2471.

[9] I.G. Bearden et al., BRAHMS Collaboration, Phys. Rev. Lett.93 (2004) 102301.

[10] M. Adamczyk et al., BRAHMS Collaboration, Nucl. Instr. and Meth.A 499 (2003) 437.

[11] I.C. Arsene et al., BRAHMS Collaboration, Phys. Rev. C 72, 014908 (2005).

[12] GEANT 3.2.1, CERN program library.

[13] V. Topor Pop et al. Phys. ReV C70 (2004)064906; X. N. Wang and M. Gyulassy, Phys. Rev. D44 (1991) 3501; S.E. Vance and M. Gyulassy, Phys. Rev. Lett.83 (1999) 1735.

[14] S. Wheaton J. Cleymans and M. Hauer, Computer Physics Communications 180 (2009) 84, hep-ph/0407174

[15] L. A. Stiles and M. Murray, arXiv:nucl-ex/0601039.

[16] F. Videbæk and O. Hansen, Phys. Rev.C 52 (1995) 2684.

[17] C. Blume for the NA49 collaboration, Proceedings from QM06, J.Phys G34 (2007) S951-954.

[18] L. Ahle et al.,E802 Collaboration, Phys. Rev.C 60 (1999) 064901.

[19] J. Barette et al., E877 Collaboration, Phys. Rev.C 62 (2000) 024901.

[20] W. Busza, A.S. Goldhaber, Phys. Lett.B 139 (1984) 235.

[21] B. Z. Kopeliovich and B. G. Zakharov, Z. Phys.C 43, (1989) 241.

[22] Y. Mehtar-Tani and G. Wolschin, Phys. Rev. Lett. 102 (2009) 182301.